Magnesium Ions Storage in Molybdenum Oxide Structures Examined as a Promising Cathode Material for Rechargeable Magnesium Batteries

Dedy Setiawan, Hyungjin Lee, Hyeri Bu, Doron Aurbach, Seung-Tae Hong,* and Munseok S. Chae*

Magnesium batteries have attracted considerable attention as a promising technology for future energy storage because of their capability to undergo multiple charging reactions. However, most oxide materials utilized as hosts for magnesium batteries do not perform well at room temperature or in nonaqueous electrolytes. Herein, a host material, $Na_{0.04}MoO_3 \cdot (H_2O)_{0.49}$ is successfully developed through the chemical reduction of alpha-MoO_3, which enables magnesium storage reaction in a 0.5 M $Mg(ClO_4)_2$/acetonitrile electrolyte at 25 °C. Electrochemical analysis reveals that the cathode material possesses a discharge capacity of 157.4 mAh g^{-1} at a 0.2 C rate. The $Na_{0.04}MoO_3 \cdot (H_2O)_{0.49}$ cathode material also exhibits a capacity retention of 93.4% after 100 cycles compared to the first cycle at a 2 C rate, with an average discharge voltage of −0.474 V versus activated carbon (≈2.16 V estimated discharge voltage vs Mg/Mg^{2+}). The study findings demonstrate, for the first time, the potential of this material as a cathode for magnesium batteries at ambient temperatures and in nonaqueous electrolytes.

1. Introduction

Lithium-ion batteries (LIBs) are currently the preferred choice for many electronic applications, such as mobile devices, tablet PCs, electric vehicles, and energy storage systems, due to their high energy and power densities.[1–3] However, instability issues, uneven lithium resource distribution, increasing demand for higher energy densities, and uncertainty regarding cost

promote continuous, worldwide efforts to develop alternative battery systems, beyond LIBs.[4] Consequently, post-LIB technologies, such as lithium–air, zinc–air, lithium–sulfur, sodium–ion, and multivalent-ion batteries, have garnered significant attention as potential solutions to address these challenges.[5–9]

The most important challenge in the field is the development of effective technologies for large energy storage (at levels of hundreds of TWh) that will allow intensive use of renewable power sources (mostly based on solar and wind energies). Such technologies should be based on the most abundant elements in the earth crust, to become cost-effective. Therefore, the development of reliable and durable secondary sodium-ion batteries and magnesium batteries is so important today. Rechargeable magnesium-ion batteries (MIBs) are hailed as a potential alternative to lithium-ion batteries (LIBs), in terms of availability of abundant elements and possible suitability for large energy storage applications, and have garnered significant attention as promising multivalent metal-ion battery technologies. These batteries offer several advantages over LIBs, including potentially lower costs owing to the higher abundance of magnesium and a higher specific capacity (both gravimetric and volumetric) of magnesium anodes in the form

D. Setiawan, H. Lee, H. Bu, S.-T. Hong
Department of Energy Science and Engineering
Daegu Gyeongbuk Institute of Science and Technology (DGIST)
Daegu 42988, Republic of Korea
E-mail: st.hong@dgist.ac.kr

D. Aurbach
Department of Chemistry
Bar-Ilan University
Ramat-Gan 5290002, Israel

S.-T. Hong
Energy Science and Engineering Research Center
Daegu Gyeongbuk Institute of Science and Technology (DGIST)
Daegu 42988, Republic of Korea

M. S. Chae
Department of Nanotechnology Engineering
Pukyong National University
Busan 48513, Republic of Korea
E-mail: mschae@pknu.ac.kr

of thin metallic foils (graphite: $777\,mAh\,cm^{-3}$, Mg: $3,833\,mAh\,cm^{-3}$), with a higher level of safety owing to the lack of dendrite formation.[10,11] Recently, metallic Sn- or Bi-based anode materials have been reported for MIBs. Several oxide host materials, such as layered oxides and polyanions, have been proposed as potential cathode candidates for MIBs.[12–26] However, oxide materials often exhibit functionality exclusively within aqueous systems or at high temperatures as host materials for multivalent-ion batteries. Water-based electrolytes have limited anodic stability, restricting the operating voltage of the host materials, as shown in Figure S1, Supporting Information. However, battery systems with multivalent ion carriers based on organic electrolyte systems have recently received considerable attention because their use can alleviate stability limitations and enable achieving battery systems working in a wide potential domains.[27]

The model of the two-dimensional layered crystal structure of molybdenum bronze, $A_xMoO_3\cdot(H_2O)_y$ (where A denotes metal ions or organic compounds), is shown in **Figure 1**a. This material acts as a host material for lithium ions in nonaqueous electrolytes.[28] Structurally, alpha-MoO_3 (which belongs to the space group Pbnm) differs slightly from molybdenum bronze $A_xMoO_3\cdot(H_2O)_y$ (which belongs to the space group A2mm), as the latter moieties have buffer layers made up of metal ions, water, or organic compounds between the MoO_3 layers. The alpha-MoO_3 lattice consists of two-dimensional metal oxide sheets attracted by van der Waals forces, and thereby they are not tightly bound together. Such structures have been shown to function as host materials for various guest ions in aqueous and nonaqueous systems, containing lithium and sodium electrolytes.[29,30] However, magnesium ions intercalation into host materials typically has slow kinetics, which makes magnesium intercalation into MoO_3 a very challenging possibility. Indeed,

Mg ions intercalation into MoO_3 has been reported only in thin molybdenum oxide films.[17] Previous studies have employed bond valence sum (BVS) calculations to assess the structural characteristics of MoO_3, highlighting the difficulties related to diffusion within the host structure (Figure S2, Supporting Information). Therefore, identifying methods for improving the electrochemical activity in MoO_3 is essential. It has been proposed that integrating a buffer layer within the MoO_3 structure, analogous to that observed in molybdenum bronze materials, could enhance the electro-chemical activity of the modified MoO_3 as a host material for magnesium-ions intercalation.

In this investigation, we examined the potential of $Na_{0.04}MoO_3\cdot(H_2O)_{0.49}$, which was synthesized via a chemical reduction process from alpha-MoO_3, as a cathode material for magnesium batteries operating at ambient temperatures (25 °C). We compared the performance of cells in organic electrolyte solutions consisting of 0.5 M $Mg(ClO_4)_2$ in acetonitrile (AN) with other electrolyte solutions containing propylene carbonate (PC) and triglyme (3G) solvents. We analyzed the electrochemical intercalation properties of magnesium ions using various techniques, including cyclic voltammetry (CV), galvanostatic analysis (charge/discharge cycling at constant currents), as well as energy dispersive X-ray spectroscopy (EDX), elemental analyses using inductively coupled plasma optical emission spectroscopy (ICP-OES), and X-ray photoelectron spectroscopy (XPS). Furthermore, we conducted structural analysis using GSAS and BVS mapping programs.

2. Results and Discussion

We synthesized $Na_{0.04}MoO_3\cdot(H_2O)_{0.49}$ by electrochemical Na extraction from $Na_{0.17}MoO_3\cdot(H_2O)_{0.49}$, initially prepared via

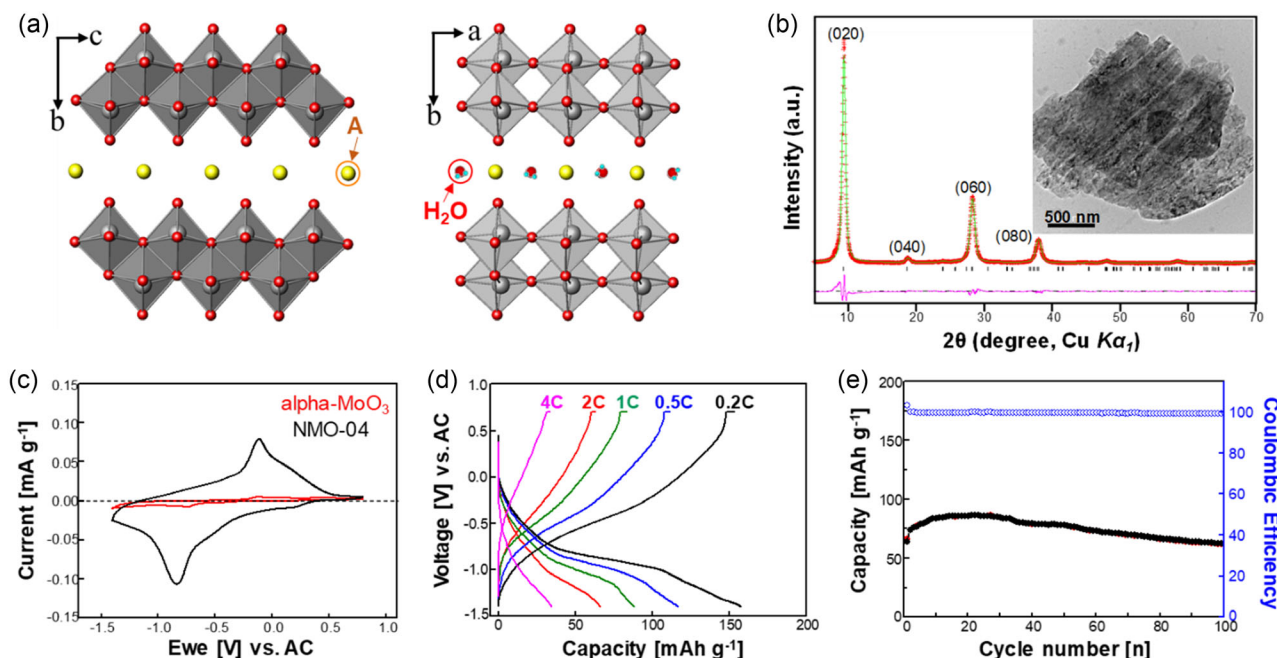**Figure 1.** a) Structure images of $A_xMoO_3\cdot y(H_2O)$. b) Powder X-ray diffraction pattern for NMO-17. c) Comparison of CV curves of NMO-04 and alpha-MoO_3 electrodes in 0.5 M $Mg(ClO_4)_2$ in AN (0.1 mV s^{-1}). d) First discharge/charge curves of the AC/NMO-04 cell with various C rates. e) Cycling performance of a representative AC/NMO-04 cell operating at 2 C rate.

**ADVANCED
SCIENCE NEWS**

www.advancedsciencenews.com

**small
structures**

www.small-structures.com

chemical reduction from alpha-MoO_3. The reduction process was performed at room temperature under an argon atmosphere using a mixed solution of Na_2MoO_4 and $Na_2S_2O_4$. The resulting $Na_{0.17}MoO_3 \cdot (H_2O)_{0.49}$ powder had a Na: Mo atomic ratio of 0.167:1.000 according to the ICP-OES analysis (Table S1, Supporting Information) and was dark blue. The water content was carefully determined using thermogravimetric analysis (TGA) (Figure S3, Supporting Information). The initial chemical formula of this material was $Na_{0.17}MoO_3 \cdot (H_2O)_{0.49}$ (referred to as NMO-17). The crystal structure of NMO-17 was analyzed using powder X-ray Rietveld refinement (Figure 1b and S4, Supporting Information), complemented by TEM imaging (inset) and electron diffraction patterns (Figure S5, Supporting Information). The refined parameters and interatomic distances are summarized in the tables provided in the Supporting Information (Table S2 and S3, Supporting Information). The crystal structure of NMO-17 is orthorhombic with a space group of A2mm, and the particle size ranges from 7 to 15 μm with a plate-like shape, as shown in the figures provided (Figure 1b and S6, Supporting Information).

Homemade two electrodes cells (Figure S7, Supporting Information) were used for the electrochemical analyses. Na-ions were extracted from the NMO-17 electrodes by charging the cells (activated carbon (AC)/0.5 M $Mg(ClO_4)_2$ in AN/NMO-17) by a 0.2 C rate up to 0.7 V (Figure S8, Supporting Information) and washing with AN solution. The C-rate is defined as the rate of charge or discharge that is completed in $(1/n)$ hours, e.g., 1 C is defined as 170.96 mA g^{-1}. Based on the charging current and water remaining in the structure, we estimate that 0.13 M of Na-ions were extracted from NMO-17, resulting in $Na_{0.04}MoO_3 \cdot (H_2O)_{0.49}$ (NMO-04). The NMO-04 phase was confirmed using various analyses, including X-ray Rietveld refinement (Figure S9, Table S4 and S5, Supporting Information), ICP-OES (Table S6, Supporting Information), and TGA (Figure S3, Supporting Information). NMO-04 electrodes were used as the electrochemical Mg^{2+} ions intercalation hosts. The first cyclic voltammetry (CV) of the NMO-04 electrodes and alpha-MoO_3 electrodes in 0.5 M $Mg(ClO_4)_2$/AN solutions showed one pair of reversible reduction and oxidation peaks at −0.834 and −0.114 V versus AC, respectively (Figure 1c). Both reduction and oxidation peak of the NMO-04 exhibits higher current density as compared to alpha-MoO_3, which emphasizes its much enhanced electrochemical activity. The estimated chemical potentials for the magnesium insertion/extraction peaks were 1.802 and 2.522 V versus Mg/Mg^{2+}, respectively, demonstrating that the buffer-layer-tuned molybdenum bronze could operate at more than 2 V (Figure S10 and S11, Supporting Information). The intercalation reaction ratio (≈70%) was observed to be higher than the adsorption reaction during the magnesium intercalation reaction (Figure S12, Supporting Information). In addition, the CVs of NMO-04 electrodes in organic electrolyte solutions containing various cations, presented in Figure S13, Supporting Information, reflect reversible insertion/extraction of other cations: Ca^{2+}, Zn^{2+}, K^+, and Na^+ into these electrodes.

Figure 1d shows the discharge/charge voltage profiles of the first cycle at various C-rates. At a rate of 0.2 C, the first discharge capacity is around 157 mAh g^{-1}, and the discharged phase can be expressed as $Mg_{0.46}Na_{0.04}MoO_3 \cdot (H_2O)_{0.49}$ (MNMO-04). The

calculated capacity of NMO-04 can be around 164 mAh g^{-1} if Mo^{6+} is fully reduced to Mo^{5+}. This corresponds to 0.96 electrons being reduced per formula unit, resulting in the insertion of a maximum of 0.48 divalent magnesium ions per unit. The observed capacity was comparable to monovalent-ions intercalation, indicating that only half of the possible sites were filled with divalent magnesium ions. However, the capacity decreases significantly with increasing C rates, with values around 117, 88, 66, and 34 mAh g^{-1} at 0.5, 1, 2, and 4 C rates, respectively.

For the first cycle, the galvanostatic intermittent titration technique analysis revealed high polarization during the magnesium ions insertion process because of the plate-shaped host materials (Figure S14, Supporting Information). Despite this, the cells based on these cathodes exhibited satisfactory cycling performance, with a specific capacity of around 66 mAh g^{-1} at the first discharge stabilizing to nearly 62 mAh g^{-1} at the 100th cycle (93.4% of the initial capacity) (Figure 1e). The capacity degradation during the initial cycles is probably caused by a small portion of the inserted magnesium ions that remain in the host structure, as demonstrated by the elemental analyses of the recharged electrodes (**Figure 2**). Some degradation in the host's structure was also observed after prolonged cycling experiments (Figure S15, Supporting Information).

It is intriguing to note that even at a lower C-rate (0.2 C), a few cycles exhibit well-maintained performance without degradation. (Figure S16a, Supporting Information). In addition, the discharge capacity of these cathodes measured in galvanostatic experiments was higher in electrolyte solutions based on AN was higher than in solutions based on PC or 3G solvents (Figure S16b, Supporting Information). These results imply that the intercalation process occurs more rapidly in AN-based solutions than in solutions comprising other solvents, probably because of variations in the solvation energy of the Mg ions with the solvent molecules (Figure S17, Supporting Information).[31] Hence, the composition of the electrolyte solutions can substantially influence the electrochemical behavior of Mg ions intercalation compounds that can be relevant for secondary magnesium battery systems. Hence, more comprehensive investigations are required to fully understand the solutions' structure and composition effect on the Mg ions intercalation mechanisms into solid hosts like transition metal oxides (that are relevant for high capacity Mg ions insertion cathodes),

Figure 2 presents the results of experiments in which NMO-04 electrodes were magnesiated and demagnesiated glavanostatically and the electrodes at different states for the experiments underwent structural and element analyses by ICP, EDS, and TEM-EDX. Figure 2a presents typical voltage profiles of a full galvanostatic cycle and the consequent change in the Mg ion content in the host due to the electrochemical process. Figure 2b presents TEM images and elements mapping (Mo and Mg) of particles taken from pristine, NMO-04, magnesiated (charged), and demagnesiated (discharged) electrodes (b 1–3 as indicated therein). The discharged samples (2) displayed consistent dispersion of Mg throughout the particles, as observed in the elemental mapping (Figure 2b). In contrast, the charged samples (3) contained only trace amounts of magnesium, indicating that the redox reaction was mainly associated with magnesium intercalation. These observations are substantiated by the structural analysis discussed below. Moreover, EDX and ICP elemental
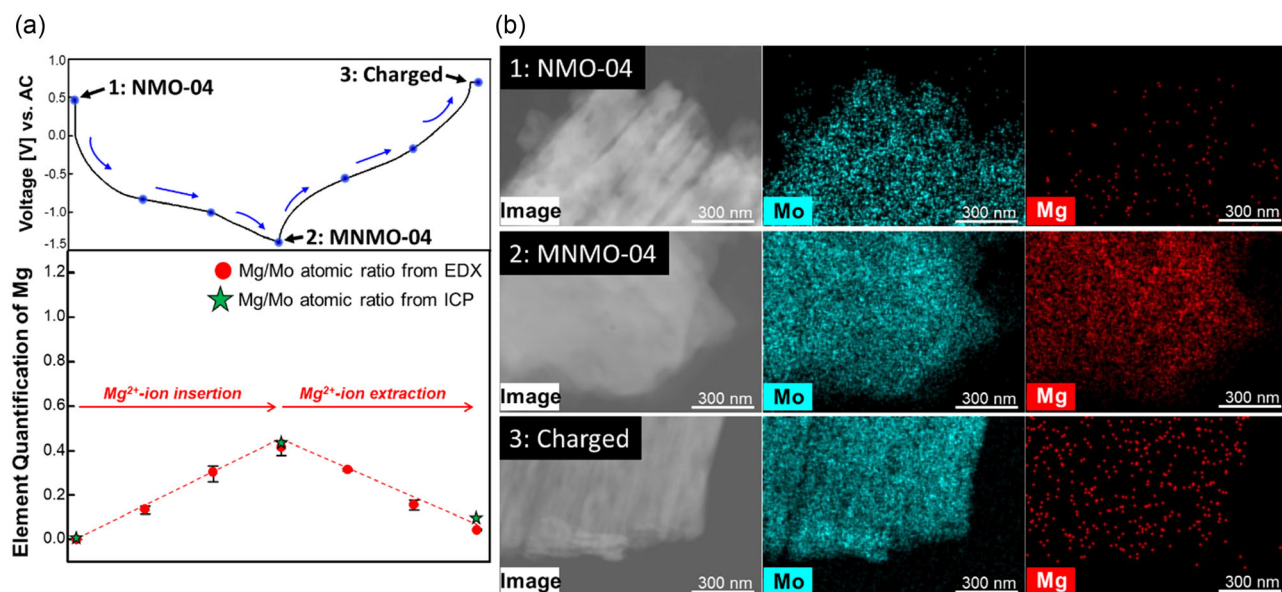
Figure 2. a) Change in x value during a discharge and charge cycling of Mg_xNMO-04 cathodes estimated from ICP and EDX elemental analyses and b) TEM-EDX elemental mappings of 1: NMO-04, 2: MNMO-04, and 3: charged MNMO-04.
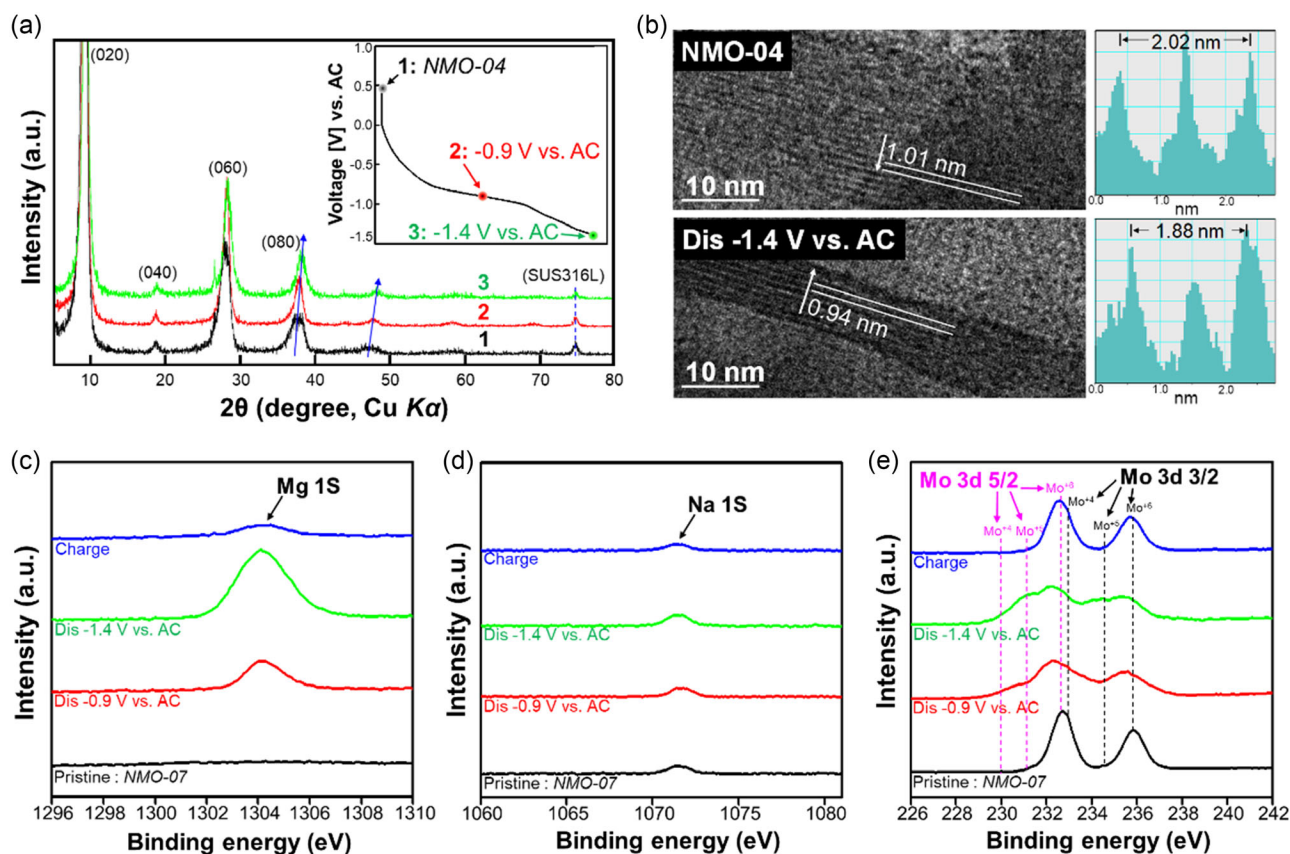

Figure 3. a) XRD patterns of (1: black) NMO-04, (2: red) discharged to −0.9 from NMO-04, (3: green) discharged to −1.4 from NMO-04. b) HR-TEM images of NMO-04 and discharged to −1.4 V versus AC. XPS survey data of c) Mo 3d, d) Mg 1s, and e) Na 1s spin-orbital.

**ADVANCED
SCIENCE NEWS**
www.advancedsciencenews.com

**small
structures**
www.small-structures.com

analyses (Tables S6 and S7, Supporting Information) provided further quantitative confirmation of the reversible Mg ions intercalation/deintercalation reactions that our NMO-04 electrodes undergo.

Figure 3a compares the ex situ powder XRD patterns of the NMO-04 electrode samples at various voltages during galvanostatic discharge and charge cycle. The patterns show slight changes with magnesium intercalation during discharging from point 1 (0.48 V) to 3 (−1.40 V). The *(0k0)* peak shifted to a higher angle than the pristine material, indicating reduced interlayer space after Mg insertion (Figure 3a). The shifting of higher angle peaks, i.e., (040) and (080), are more significant compared to lower angle peaks due to smaller interlayer distance of, which are affected more by the change of unit cell parameters. The unit cell parameter b decreased by 1.7% (from 19.191 to 18.862 Å). The formation of the MNMO-04 (magnesiated) phase was confirmed by Rietveld refinement (Figure S18, Tables S8, and S9, Supporting Information), TG (Figure S3, Supporting Information), and ICP (Table S6, Supporting Information) analyses. The HRTEM image in Figure 3b clearly shows a decreasing (020) lattice parameter after Mg insertion. The XPS profiles in the magnesium, sodium, and molybdenum ranges are shown in Figure 3c–e. The spectra show that the magnesium ions are inserted into the NMO-04 phase, reducing some Mo and thus generating double peaks of Mo(V) $3d_{5/2}$ and Mo(V) $3d_{3/2}$ at 231.5 and 234.7 eV, respectively (Figure 3e), along with a new Mg 1s peak (Figure 3c) and Na 1s peak (Figure 3d). Although as observed in XPS the Na 1s intensity appears to be constant,

the ICP-OES (Table S6, Supporting Information) reveals that Na contents during discharge and charge are reduced although insignificant. This signifies that there is a possible exchange reaction between Mg^{2+} and Na^+ during discharge and charge. Therefore, we can also observe a gradual increase in NMO capacity at initial cycles due to these activation process (Figure 1e).

The TGA results in Figure S3, Supporting Information, confirm the amount of crystal water present during the magnesium insertion and extraction processes. Crystal water did not participate in the reaction. In addition to the XRD structural analysis results, structural changes were observed in parameter *b*. Particularly, *b* increased upon sodium ions extraction and decreased upon magnesium ions insertion. A schematic illustration of these reactions is shown in **Figure 4**a.

We used the bond valence sum mapping (BVSM) method to better understand the magnesium conduction pathways through a valence program. The atoms in Figure 4b,c retain their original orientation and arrangement, with oxygen atoms represented by red balls and molybdenum atoms represented by grey balls. To check the refined crystal structure, we used an empirical expression for the bond valence, widely adopted to estimate the valences in inorganic solids. BVSM is represented by the isosurfaces at $|\Delta v| = 0.15$ valence unit (vu) for magnesium ions. The (100) and (001) directions' views reveal magnesium ions diffusion channels parallel to the planes. Notably, these channels exist only along two crystallographic axes (the ac plane and not in the b direction). Moreover, by comparing the diffusion pathways
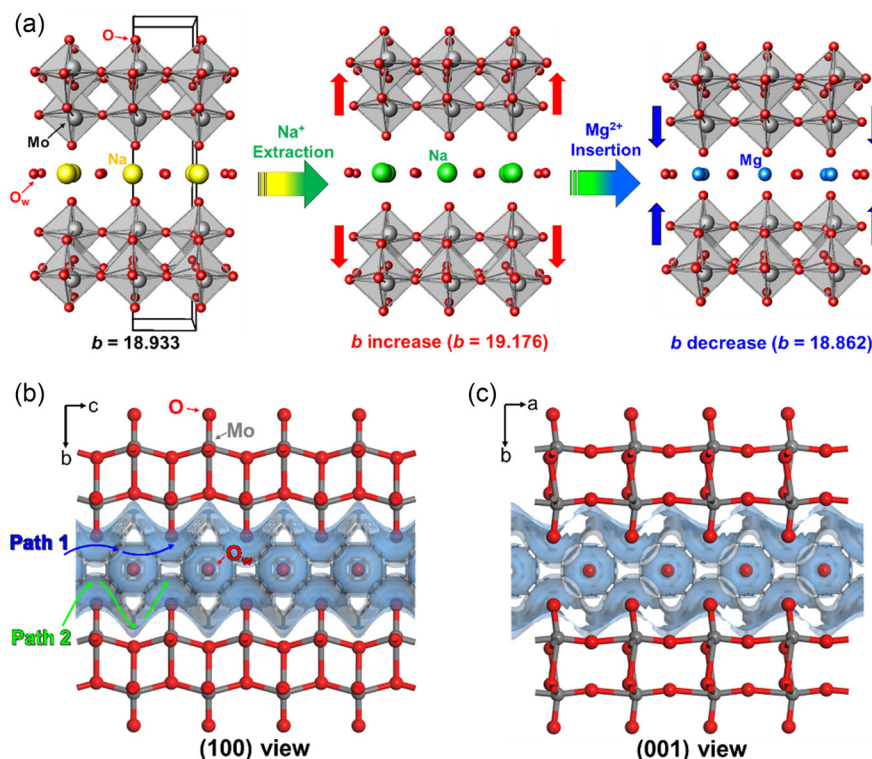

Figure 4. a) A schematic illustration of the redox reaction of NMO-04 by structural and elemental analyses. 3D bond valence differences map isosurfaces (sky-blue color) for MNMO-04 on the b) (l00) and the c) (00 L) directions with the isosurfaces of |0.15| vu, respectively.
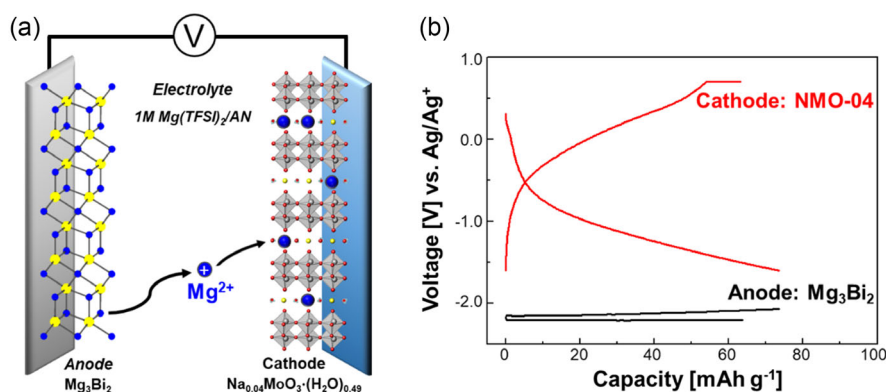
2300228 (5 of 7)

Figure 5. a) A schematic illustration of Mg ion battery prototypes comprising Mg_3Bi_2 and NMO-04 electrodes. b) The initial galvanostatic voltage profiles of a full cell with an electrolyte solution containing 1 M $Mg(TFSI)_2$ in AN operating at 0.5 C.

involving the crystal water (path 1-blue) and those involving the MoO_3 surface (path 2-green), we confirmed that the diffusion pathways involving crystal water were more connected. The BVSM results demonstrate the 2D network of magnesium ion diffusion pathways along the a- and c-axes, which support the notion that the reaction-favoring path 1 is the preferred pathway. Activation of diffusion pathways through crystal water becomes feasible in flexible and layered crystal structures, thereby creating additional diffusion routes with expanded interlayer spacings. However, in the context of structurally rigid spinel and other materials with 1D properties, the presence of water molecules could potentially obstruct their diffusion pathways.

To investigate the performance of magnesium-ion battery prototypes based on the molybdenum oxide bronze cathodes described herein, we constructed full cells using Mg_3Bi_2 alloy anodes, NMO-04 cathodes, and 1 M $Mg(TFSI)_2$/AN electrolyte solutions. This electrochemical system is shown in **Figure 5**a. The Mg_3Bi_2 anode was synthesized via ball milling and mixed with conductive carbon and a PVDF binder (7:2:1 w/w) before being coated onto a stainless-steel foil. The Mg_3Bi_2 powder appeared gray with submicron-sized particles (Figures S19 and S20, Supporting Information). AN was selected as the electrolyte solution's solvent owing to the high ionic conductivity of the Mg^{2+} ion in the obtained electrolyte. The NMO-04/Mg_3Bi_2 full cells were composed of negative and positive electrodes in a mass ratio of 3:1, providing positive electrode-limiting cells. Figure 5b shows the reversible discharge-charge voltage profiles of each electrode in these cells, measured using three-electrode cells with Ag/Ag^+-based reference electrodes. The negative electrodes exhibited flat voltage profiles at -2.16 V. In comparison, the positive electrodes were discharged to -1.00 V, showing specific capacities around 73 mAh g^{-1}, and then charged up to 0.70 V at a 0.5 C rate, indicating the successful operation of these new magnesium-ion battery systems. However, the limited functionality of the cell is attributed to the inadequate electrolyte combination, specifically $Mg(TFSI)_2$/AN. To enhance overall cell performance, further research into suitable electrolyte compositions is imperative and forms a pivotal aspect of our future research scope.

3. Conculsion

This study represents an advancement in developing rechargeable magnesium-ion batteries (MIBs) operable at ambient temperatures. A new oxide host material, $Na_{0.04}MoO_3 \cdot (H_2O)_{0.49}$, was synthesized using chemical reduction methods and characterized as Mg^{2+} ions host material through electrochemical, elemental, and structural analyses. The insertion of Na and crystal water leads to the structural transformation of alpha-MoO_3 into a buffer layers structure which is beneficial for Mg^{2+} diffusion. This work also characterized full-cell MIB systems with Mg_3Bi_2 anodes and $Na_{0.04}MoO_3 \cdot (H_2O)_{0.49}$ cathodes in 1M $Mg(TFSI)_2$/AN electrolyte solutions. Although challenges remain in optimizing the anodes and the electrolyte solutions, this study demonstrates the feasibility of using this unique oxide host material in nonaqueous MIBs at ambient temperatures. These findings could motivate further work in the search for new host materials via simple chemical reduction methods that may offer reasonably high capacities and discharge voltages for MIB technology.

Supporting Information

Supporting Information is available from the Wiley Online Library or from the author.

Acknowledgements

Conflict of Interest

The authors declare no conflict of interest.

[1] M. Armand, J.-M. Tarascon, *Nature* **2008**, *451*, 652.

[2] P. G. Bruce, B. Scrosati, J. Tarascon, *Angew. Chem. Int. Ed.* **2008**, *47*, 2930.

[3] K. Amine, R. Kanno, Y. Tzeng, *MRS Bull* **2014**, *39*, 395.

[4] K. T. Lee, S. Jeong, J. Cho, *Acc. Chem. Res.* **2013**, *46*, 1161.

[5] J.-M. Tarascon, *Philos. Trans. R. Soc., A* **2010**, *368*, 3227.

[6] P. Canepa, G. S. Gautam, D. C. Hannah, R. Malik, M. Liu, K. G. Gallagher, K. A. Persson, G. Ceder, *Chem. Rev.* **2017**, *117*, 4287.

[7] C. Xu, B. Li, H. Du, F. Kang, *Angew. Chem. Int. Ed.* **2012**, *51*, 933.

[8] M. M. Thackeray, C. Wolverton, E. D. Isaacs, *Energy Environ. Sci.* **2012**, *5*, 7854.

[9] P. G. Bruce, S. A. Freunberger, L. J. Hardwick, J.-M. Tarascon, *Nat. Mater.* **2012**, *11*, 19.

[10] M. Matsui, *J. Power Sources* **2011**, *196*, 7048.

[11] J. Muldoon, C. B. Bucur, T. Gregory, *Angew. Chem. Int. Ed.* **2017**, *56*, 12064.

[12] L. R. Parent, Y. Cheng, P. V. Sushko, Y. Shao, J. Liu, C.-M. Wang, N. D. Browning, *Nano Lett.* **2015**, *15*, 1177.

[13] Y. Shao, M. Gu, X. Li, Z. Nie, P. Zuo, G. Li, T. Liu, J. Xiao, Y. Cheng, C. Wang, J.-G. Zhang, J. Liu, *Nano Lett.* **2014**, *14*, 255.

[14] C. Ling, R. Zhang, T. S. Arthur, F. Mizuno, *Chem. Mater.* **2015**, *27*, 5799.

[15] X. Sun, V. Duffort, B. L. Mehdi, N. D. Browning, L. F. Nazar, *Chem. Mater.* **2016**, *28*, 534.

[16] C. Kim, P. J. Phillips, B. Key, T. Yi, D. Nordlund, Y. Yu, R. D. Bayliss, S. Han, M. He, Z. Zhang, A. K. Burrell, R. F. Klie, J. Cabana, *Adv. Mater.* **2015**, *27*, 3377.

[17] G. Gershinsky, H. D. Yoo, Y. Gofer, D. Aurbach, *Langmuir* **2013**, *29*, 10964.

[18] S. Tepavcevic, Y. Liu, D. Zhou, B. Lai, J. Maser, X. Zuo, H. Chan, P. Král, C. S. Johnson, V. Stamenkovic, N. M. Markovic, and T. Rajh, *ACS Nano* **2015**, *9*, 8194.

[19] P. Novák, V. Shklover, R. Nesper, *Z. Phys. Chem.* **1994**, *185*, 51.

[20] Z.-D. Huang, T. Masese, Y. Orikasa, T. Mori, K. Yamamoto, *RSC Adv.* **2014**, *5*, 8598.

[21] J. Zeng, Y. Yang, S. Lai, J. Huang, Y. Zhang, J. Wang, J. Zhao, *Chem. Eur. J.* **2017**, *23*, 16898.

[22] W. Kaveevivitchai, A. J. Jacobson, *Chem. Mater.* **2016**, *28*, 4593.

[23] J. T. Incorvati, L. F. Wan, B. Key, D. Zhou, C. Liao, L. Fuoco, M. Holland, H. Wang, D. Prendergast, K. R. Poeppelmeier, J. T. Vaughey, *Chem. Mater.* **2016**, *28*, 17.

[24] T. E. Sutto, T. T. Duncan, *Electrochim Acta* **2012**, *79*, 170.

[25] Y. Orikasa, T. Masese, Y. Koyama, T. Mori, M. Hattori, K. Yamamoto, T. Okado, Z.-D. Huang, T. Minato, C. Tassel, J. Kim, Y. Kobayashi, T. Abe, H. Kageyama, Y. Uchimoto, *Sci. Rep.* **2014**, *4*, 5622.

[26] T. Mori, T. Masese, Y. Orikasa, Z.-D. Huang, T. Okado, J. Kim, Y. Uchimoto, *Phys. Chem. Chem. Phys.* **2016**, *18*, 13524.

[27] A. L. Lipson, S.-D. Han, S. Kim, B. Pan, N. Sa, C. Liao, T. T. Fister, A. K. Burrell, J. T. Vaughey, B. J. Ingram, *J. Power Sources* **2016**, *325*, 646.

[28] T. A. Kerr, H. Wu, L. F. Nazar, *Chem. Mater.* **1996**, *8*, 2005.

[29] J. S. Chen, Y. L. Cheah, S. Madhavi, X. W. Lou, *J. Phys. Chem. C* **2010**, *114*, 8675.

[30] Y. Dong, X. Xu, X. Li, C. Han, K. Zhao, L. Zhang, C. Niu, Z. Huang, L. Mai, *Nano Energy* **2015**, *15*, 145.

[31] M. Okoshi, Y. Yamada, S. Komaba, A. Yamada, H. Nakai, *J. Electrochem. Soc.* **2017**, *164*, A54.